Improving sensitivity of a miniaturized label-free electrochemical biosensor using zigzag electrodes

Yi-Ching Kuo, Chih-Kung Lee, Chih-Ting Lin

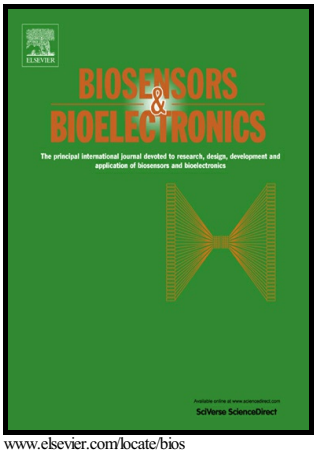

www.elsevier.com/locate/bios

PII: S0956-5663(17)30794-7
DOI: http://dx.doi.org/10.1016/j.bios.2017.11.065
Reference: BIOS10141

To appear in: *Biosensors and Bioelectronic*

Received date: 7 August 2017
Revised date: 22 November 2017
Accepted date: 24 November 2017

Cite this article as: Yi-Ching Kuo, Chih-Kung Lee and Chih-Ting Lin, Improving sensitivity of a miniaturized label-free electrochemical biosensor using zigzag electrodes, *Biosensors and Bioelectronic* http://dx.doi.org/10.1016/j.bios.2017.11.065

Improving sensitivity of a miniaturized label-free electrochemical biosensor using zigzag electrodes

Yi-Ching Kuo,[a] Chih-Kung Lee,[a,b,c,*] Chih-Ting Lin[c]

[a]National Taiwan University, Engineering Science & Ocean Engineering, Taipei 10617, Taiwan

[b]National Taiwan University, Institute of Applied Mechanics, Taipei 10617, Taiwan

[c]National Taiwan University, Graduate Institute of Electronics Engineering, Taipei 10617, Taiwan

[*]**Correspondence to**: National Taiwan University, Institute of Applied Mechanics, No. 1, Sec. 4, Roosevelt Road, Taipei, 10617 Taiwan; Tel.: (+886) 2 3366-5645; fax: (+886) 2 3366-5654; cklee@ntumems.net

Abstract:

Cardiovascular disease (CVD) is a leading cause of death among chronic diseases worldwide. Therefore, it is important to be able to detect CVD biomarkers early so that patients can be diagnosed properly and begin treatment as soon as possible. To detect biomarkers more conveniently, point-of-care (PoC) biosensors, which are easy to use and are of low cost, are becoming even more necessary. This paper focuses on developing a label-free electrochemical biosensor with high sensitivity for PoC applications to detect CVD biomarkers such as S100 beta proteins and C-reactive proteins (CRP).

To meet the requirements of a PoC application and to improve the measurement sensitivity for detection purposes, a three-electrode configuration was miniaturized and fitted onto a biochip. Computer simulation of an electrolyte current density was used to investigate several potential effective possibilities. It was found that an electrolyte current density at an edge tip structure near the working electrode (WE) and counter electrode (CE) was higher than at other locations. A zigzag structure was then designed at the edge near the WE and CE positions. With this design, we can obtain a higher total electrolyte current. This newly-designed biochip was then used to measure the electrochemical feature. It was found that the measurement efficiency was also improved using this newly designed biochip.

Keywords:

Point-of-care biosensor, biochip, zigzag electrode, cardiovascular disease, electrochemical.

1. Introduction

The proportion of people aged 60 and above has been increasing year after year. To allow these elderly people to live longer and healthier, a device which can monitor the body at anytime and anywhere is ideal. To meet such a requirement, the device must have properties

such as small size, low cost, portability, and can provide enough sensitivity. Moreover, in recent years, non-communicable diseases have resulted in about 68% of all deaths around the world every year. Among these deaths, about 46% were deaths from cardiovascular diseases (CVD) [1] which has been ranked as the first cause of death in Western countries for many years already and has been ranked as one of the top three causes of death in Taiwan over the last two decades. Early screening of CVD and then providing suitable care when diagnosed are becoming two important issues for these countries. Therefore, the development of a point-of-care (PoC) CVD biosensor is becoming a necessary trend. CVD can be diagnosed by detecting the CVD biomarkers. S100 beta protein has been evaluated as a biomarker in the prognosis of chronic heart failure [2]. Moreover, although CRP is not a cardiac-specific biomarker, several studies have shown that heart patients with higher detected levels of CRP had a worse prognosis [2].

A biosensor [3,4] is generally defined as an analytical device that is made up of a bio-receptor, a transducer, and a signal processing display. Bio-receptors have been used as probes to capture analytes. A transducer converts a bio-signal into a measurable signal. Finally, the measured signal is amplified, processed, and displayed by an electronic system through a signal processing display. According to the basic principles of signal transduction, a transducer can be divided into three types: optical [5,6], mechanical [7-9], and electrochemical (e.g. field-effect transistors) [10-12]. Of the various types of biosensors, an electrochemical biosensor is most commonly used in micro/nano technologies in PoC applications. They have been commercialized for clinical, industrial, and environmental applications fields due to advantages such as being label-free, low cost, compact in size, and possessing a rapid response time [13], which makes it suitable for PoC applications. In particular, electrochemical impedance spectroscopy (EIS) can monitor the changes of capacitance (non-faradaic process) or electronic transfer resistance (faradaic process) to better understand the interaction on the sensing surface. For non-faradaic processes, the bio-molecules interactions are measured according to the insulating properties of biological molecules. However, the measurement method of non-faradaic processes has a major risk in that the defects on the modified sensor surface may result in the insulator of the uniformly distributed layer to be imperfect and then indirectly generates a leakage current. The sensor sensitivity may thus be affected in that way. On the other hand, a faradaic process, which was used in this article, utilizes an oxidation/reduction of the redox species to measure the faradaic current. This faradaic current can be affected by steric hindrance (e.g. the insulating properties of the bio-molecules) and electrostatic attraction/repulsion (e.g. the charge between the bio-molecules and the electrolyte) [14]. These characteristics can make the faradaic process suitable for detecting various bio-molecules [15,16] and are thus thought to be a powerful tool for biological detection.

Over the past two decades, much research has been focused on improving the sensitivity

and detection limit of electrochemical impedance biosensors to further realize PoC applications. These methods include labeling [17], improving the linker layer [12], adjusting the experimental architecture and parameters [18], reforming the electrode structure [19-22], and so on. In 1988, with regard to research on reforming the electrode structure, K. Aoki *et al*. [23] proposed a current equation for an interdigitate electrode in electrochemical measurements. They assumed that the reaction rate was mass transport limited where the analyte can only move via diffusion and that the widths of the generator and collector electrodes are equal. The equation is shown below as follows:

$$I = nFDC^{*}mb\left\{0.637ln\left[2.55\left(1+\frac{w}{w_g}\right)\right]-\frac{0.19}{\left(1+\frac{w}{w_g}\right)^{2}}\right\}$$

It indicated that the electrochemical current is related to the number of charge transfers (n), the Faraday constant (F), the constant for both the oxidized and reduced species (D), the bulk analyte concentration (C^{*}), the number of the electrode pairs (m), the electrode length (b), the electrode width (w), and the gap width (w_g). Since then, further research has improved their sensing signal by tuning the parameters in this equation, which are generally the electrode width, the number of electrodes, the gap width, and the electrode length [24]. Moreover, some three-dimensional electrodes were also developed. Due to the increased effective electrode surface area and the decreased diffusion distance between the sensing electrodes, the sensing signal can be significantly improved. Our group also worked on research to reform the electrode structure. We improved the electrochemical measurement sensitivity for detecting the CVD biomarker, S100, by 46% by lengthening the edges near the working electrode (WE) and counter electrode (CE) of the biochip from 21.6 mm to 43.95 mm [25]. To lengthen the edges, the electrodes were designed to have meso-scale rectangular interdigitated structures.

In this study, based on a previous study done by our group, we further enhanced the quality of our biosensor for other various detections of PoC applications in future. The structure effect at the edge of the WE and CE was investigated using computer simulation to look into the possibility of further improving the measurement efficiency. According to the simulation results, we looked into the improving measurement efficiency by adding two kinds of micro-scale structures, a semi-circle and a triangle, to the meso-scale rectangular interdigitated electrode edges near the WE and CE without changing the areas of the WE and CE by maintaining the gap between the two electrodes. Our results showed an increased improvement in the electrochemical measurement sensitivity for detecting CVD biomarkers, S100 beta protein and CRP.

2. Experimental Details

2.1 Chemicals, bio-molecules, and solutions

The phosphate buffered saline (PBS) was purchased from Uni-Onward Corp., Taiwan. Before the electrochemical experiment, a 1×PBS, pH 7.4 was filtered through a 0.22 μm membrane. Potassium hexacyanoferrate(III) ($K_3Fe(CN)_6$, P8131) and potassium hexacyanoferrate(II) trihydrate ($K_4Fe(CN)_6 \cdot 3H_2O$, P3289), used as electrolytes, were purchased from Sigma-Aldrich. The 4-ATP (422967) and cysteamine (M9768) were purchased from Aldrich. As linkers, the 4-ATP was dissolved in a 99.8% ethanol solution to 5 mM, and the cysteamine was dissolved with D.I. water to 5 mM. The linkers were prepared immediately before usage. Glutaraldehyde (G6257) which was used as the activation reagent was purchased from Sigma-Aldrich. Before use, the glutaraldehyde was diluted with 99.8% ethanol to 4%. The blocking reagent, ethanolamine hydrochloride (ETA-HCl, E6133), was purchased from Sigma-Aldrich. Before usage, the ETA-HCl was dissolved with D.I. water purified through a Milli-Q system (Millpore) to 1 M and its pH adjusted 8.2. Table 1(a) shows the molecular weight and structure of the 4-ATP, cysteamine, glutaraldehyde, and ETA. For regeneration, glycine (50046) obtained from Sigma was used. Before use, the glycine was dissolved by D.I. water to 10 mM.

Two kinds of CVD biomarkers, S100 beta protein and CRP, were used as the model protein to verify the improved electrochemical measurements. The S100 beta protein (ab82734), S100 beta antibody (ab11178), CRP (ab51784), and CRP antibody (ab13426) were all purchased from abcam. Table 1(b) shows the detailed information of the target protein, S100 beta protein and CRP. Bovine serum albumin (BSA, A7906) used for blocking was purchased from Sigma-Aldrich. Before usage, the BSA was dissolved by 1×PBS to 15.15 μM. All the bio-molecules were diluted with 1×PBS, pH 7.4 before usage.

2.2 Biochip and microfluidic system for electrochemical measurements

An electrochemical three-electrode system was used in this study. Three kinds of electrodes, consisting of a WE, a CE, and a reference electrode (RE), were laid out onto a glass substrate of size 20 mm by 25 mm which was designated as a biochip. The biochip was fabricated by following a standard lithography process. Titanium (20 nm) and pure gold (150 nm) were evaporated on the glass substrate into a specific pattern to form the three electrodes. The titanium was used to connect the gold and the glass substrate. The areas of the WE, CE, and RE were 10.7 mm^2, 11.54 mm^2, and 1.2 mm^2, respectively. The gap among the three electrodes was 200 μm. Three kinds of biochips, which conformed to the conditions described above, were investigated in this study. In the first biochip, which we called the interdigitate biochip, the WE and the CE alternated into the interdigitate form at the detection area. Based on the interdigitate biochip, a semi-circle structure and a triangular structure were added to the edge near the WE and the CE with a fixed 200 μm horizontal gap to form the interdigitate-semicircle biochip and the interdigitated-zigzag biochip, respectively. Figure

1(a)(b)(c) shows the detailed electrode dimensions. The electrochemical measurement set-up used in this study is shown in Data in Brief Figure 2.

2.3 Computer simulation

The distributions of the electrolyte current density on the electrodes were computer simulated using a finite-element software model (COMSOL 4.4). There were two stages of simulations performed. In the first stage of the simulation, two simple simulation models were simulated to investigate the potential effective conditions. One simulation model contained a single semi-circle structure at the edge of the WE, and 200 μm gap was set between the CE and the round tip of the WE. The other one contained a single triangular structure at the edge of the WE, and 200 μm gap was set between the CE and the triangular tip of the WE. Figure 2(a)(c) shows the schema diagrams. In both of the two simulation models, the top and bottom sides of the electrolyte were set as the insulation layer. In the second stage of the simulation, the X-Y cross section of the whole detection area of the biochip was chosen for the simulation. The simulation model of the interdigitate biochip is illustrated in Figure 3(b). All the boundary sides (top, bottom, left, and right sides) were set as the insulation layer. Moreover, the semi-circle structure and triangular structures were also added at the edge of the WE and CE in this simulation stage to simulate the interdigitate-semicircle biochip and interdigitate-zigzag biochip, respectively. Except for the factors studied in this article, other variables (labeled in Figure 3(b)) which might affect the electrolyte current were all fixed. In both of the two simulation stages, materials of all the electrodes used were gold. Water, whose electrolyte conductivity was set to 0.01 S/m, was chosen as the medium surrounding all the electrodes to simulate the electrochemical electrolyte (1×PBS with 1 mM $K_3Fe(CN)_6$ and 1 mM $K_4Fe(CN)_6$). The voltage difference applied to the WE and CE was 5 mV to correlate with the electrochemical measurements. For simplification, a two-dimensional space dimension was selected. The physical model used was an electrochemistry secondary current distribution, and the study type was stationary.

2.4 Modification of gold electrode for antibody-antigen interaction

The biochip was immersed in a piranha solution (96% H_2SO_4 : 30% H_2O_2 = 3:1 by volume) for 4 min, followed by D.I. water under ultrasonic cleaning for 3 minutes. The biochip was then dried with a N_2 stream. After the cleaning, the biochip except for the reference electrode, was immersed in 4-ATP for 2 hours at room temperature. The biochip was then rinsed with ethanol and D.I. water and again dried using a N_2 stream. The 4-ATP modified gold electrode was then reacted with the glutaraldehyde at a flow rate of 5 μl/min for 15 min to form an aldehyde surface for protein binding. After modification by the glutaraldehyde, the NH_2 functional group of the antibody was able to bind to the aldehyde of

the modified electrode to capture the antigen. Then, a 111 nM antibody was added to the modified gold electrodes at a flow rate of 5 μl/min for 20 min. To avoid unwanted binding between the aldehyde, which was not replaced by the antibody, and the NH_2 functional group of antigen, a 1 M ETA-HCl solution at pH 8.2 and a 15.15 μM BSA were introduced respectively at a flow rate of 5 μl/min for 6 min to block the unreacted aldehyde group. Then, the protein at different concentrations was prepared with 1×PBS at pH 7.4, which was added to interact with the antibody at a flow rate of 25 μl/min for 5 min. To regenerate the surface, a 10 mM glycine at an appropriate pH value was used at a flow rate of 25 μl/min for 30 sec. The steps described above are shown in Figure 5(a). All the reaction conditions described above were determined by using Biacore T200. The detailed experimental data are shown in Data in Brief Figure 3 and Data in Brief Figure 4.

2.5 Electrochemical measurement methods

For the electrochemical measurements, the supporting electrolyte was a 1×PBS, pH 7.4 with 1 mM $K_3Fe(CN)_6$ and 1 mM $K_4Fe(CN)_6$ redox species. EIS performed using a CHI614D electrochemical analyzer (CH Instrument) monitored the interaction between the antibody and antigen. A DC bias voltage was set at the open circuit potential of the redox species. An AC perturbation was set small (5 mV) to keep the linearity between the voltage and current and to avoid the probe-target binding being disturbed. The frequency of the AC perturbation was set at 1 Hz to 100 kHz. The measured impedance data was then fitted with a Randles equivalent circuit model (Figure 5(b)) using ZView software (V3.2, Scribner Associates, Inc., North Carolina, USA). By fitting the impedance data, the parameters such as R_s, R_{et}, Z_w, and C_{dl} could be determined. Generally, in a faradaic process, the circuit element most commonly used to reveal affinity binding is R_{et}.

3. Results and Discussions

3.1 Computer simulation

To improve the sensitivity of the biochip in electrochemical measurements, the distribution of the electrolyte current density on the electrodes was simulated. In the first stage of the simulation, a single structure at the edge of the WE near the CE was first simulated. The results are shown in Figure 2. A higher electrolyte current density, which is about 1.66 $A/m^{2,}$ is shown at the triangular tip. The electrolyte current density declined sharply along the path away from the triangular tip. It is half way down on the electrode about 1.42 μm away from the triangular tip and shows a reading of about 0.29 A/m^2 on the electrode 20 μm away from the triangular tip. In contrast, the electrolyte current density at the round tip was about 0.44 A/m^2. It gradually slowed down and showed a reading of about 0.29 A/m^2 on the electrode 20 μm away from the round tip. The electrolyte current density on the electrode 20 μm away from the triangular tip is almost the same as the electrode 20 μm

away from the round tip, but at the triangular tip, it was about 3.77 times larger than that found at the round tip.

Based on the findings described above, in the second stage of the simulation, the semi-circle and triangular structures were added at the edges of the WE and CE without changing the electrode areas of the WE, CE, RE, and the electrolyte. The simulation results are shown in Figure 3(c)(d)(e). The electrolyte current density was transformed into an electrolyte current by multiplying it by the area of the electrolyte. The electrolyte current of the interdigitate biochip was 2.138 μA. When the semi-circle structures are added to the electrode edge of the interdigitate biochip, the electrolyte current increased from 2.138 μA to 2.156 μA (Figure 3(d)). The rate increase was about 0.84%. On the other hand, when the triangular structures are added to the electrode edge of the interdigitate biochip, the electrolyte current increased from 2.138 μA to 2.269 μA (Figure 3(e)). The rate increase was about 6.13%.

Although the gap was fixed at 200 μm in each horizontal line, the paths of the current flow could have been shorter due to the structures at the electrode edge. The shortest path between the WE and CE in the interdigitate-semicircle biochip was 150 μm (from the round tip of the WE to the round tip of the CE), and was 111.8 μm (from the triangular tip of the WE to the triangular tip of the CE) in the interdigitate-zigzag biochip (Figure 1(b)(c)). To confirm that the increased degree of the electrolyte current was mainly from the structures or the shortened path of the current flow, the simulation of the interdigitate biochip with a 150 μm gap was first performed to compare with the interdigitate-semicircle biochip (Figure 1(d)). The results showed that the electrolyte current was 2.179 μA. The rate increase from the 200 μm gap to the 150 μm gap was about 1.9%. This rate increase was larger than that from the interdigitate biochip to the interdigitate-semicircle biochip. It was deduced that the rate increase of the electrolyte current by adding a semi-circle structure on the electrode edge may be mainly from the shortened current flow path. The simulation of the interdigitate biochip with a 111.8 μm gap was also performed to compare to the interdigitate-zigzag biochip (Figure 1(e)). Results show that the electrolyte current for the interdigitate biochip with a 111.8 μm gap was 2.155 μA. The rate increase from the 200 μm gap to the 111.8 μm gap was about 0.08%. This rate increase was smaller than that from the interdigitate biochip to the interdigitate-zigzag biochip. Even though the gap between the WE and CE was reduced to the shortest distance, the electrolyte current was still lower than that of the interdigitate-zigzag biochip. It was shown that adding zigzag structures to an electrode edge can significantly increase electrolyte current, and this increase is from a point effect and not as a result of a shorter current flow path.

Moreover, a three-dimensional space dimension computer simulation was performed to obtain the spatial information of the point effect. A part of the interdigitate-zigzag biochip was chosen for the simulation. The simulation model is shown in Figure 4(a). Both of the

two electrodes were 200 nm in height. The electrolyte, which was 400 μm in length, 150 μm in width, and 0.4 μm in height, covered the electrodes. The voltage difference applied to the two electrodes was 5 mV to correlate with the experimental measurements. Other simulation conditions were the same as the simulation conditions described above. The results of the distribution of the electrolyte current density on the electrodes is shown in Figure 4(b)(c), which show that a higher electrolyte current density appears at the tip of the triangular prism between the two electrodes. It was further verified that the point effect indeed existed at the tip of the triangular structure.

3.2 Sensitivity improvement using our biochip design

We know that a charge distribution of a conductor surface is dependent upon the surface topography. We also know that more charges accumulate on sharper surfaces, resulting in a larger electrical field and at a higher current density. In our electrochemical measurements of a three-electrode cell, the current flowed through the WE and CE. A higher electrolyte current density between the WE and CE represented a higher current flow. Therefore, there was a high current flow with a triangular tip. Assuming that bio-molecules on average bind at the edges of electrodes, the probability of the bio-molecules being measured will be higher using a triangular tip than with a round tip, which we found to be 3.77 times higher. Based on this effect, the sensing signal resulting from the bio-molecules with different concentrations can be enhanced. Moreover, when the structures were added at the electrode edge of the interdigitate biochip, the edge of the WE and CE were lengthened. The edges near the WE and CE in the interdigitate biochip, interdigitate-semicircle biochip, and interdigitate-zigzag biochip were 43.95 mm, 61.94 mm, and 82.3 mm, respectively. Based on the conclusions in previously published papers [25], the electrochemical measurement sensitivity can be improved with a lengthened edge between the WE and CE. Therefore, adding a semi-circle and triangular structure at the edges near the WE and CE can be expected to further enhance the electrochemical measurement sensitivity.

3.3 Electrochemical measurements

To determine the DC potential of the EIS, a CV measurement of the bare electrodes was performed first, and a 0 V formal potential was obtained. We then set the DC potential of the EIS to 0 V. The antibody-antigen interaction measurement using the EIS was repeated three times.

The impedance data of the 4-ATP/glutaraldehyde/antiS100/ETA&BSA modified electrode after the addition of the S100 beta protein at different concentrations in the Nyquist form for interdigitate biochip, interdigitate-semicircle biochip, and interdigitate-zigzag biochip are shown in Data in Brief Figure 1(a), Data in Brief Figure 1(b), and Data in Brief Figure 1(c), respectively. When the concentration of the S100 beta protein increased, the

interaction between the S100 beta antibody and S100 beta protein also increased, resulting in a larger steric hindrance. Moreover, the charge of the S100 beta protein whose isoelectric point was 4.52, confirms that there is an electrostatic repulsive force between the S100 beta protein and the negatively charged redox species in a 1×PBS at pH 7.4. Based on these two effects, the impedance change became more dramatic. To quantify the protein, we defined a parameter:

$$\Delta R_{et} = R_{et(Protein)} - R_{et(Blocking)}$$

where $R_{et(Protein)}$ is the R_{et} value measured after adding the protein at different concentrations, and $R_{et(Blocking)}$ represents the R_{et} value before the addition of the protein. Figure 5(c) shows a good logarithmic linear relationship, with a regression coefficient of 0.9789, 0.9885, and 0.9861 between the R_{et} and a logarithm of the S100 beta protein concentrations that was found to be in the range between 27 pM (10 ng/ml) and 270 nM (10 μg/ml) in all three biochips. The slopes of the trend line equations for the interdigitate biochip, interdigitate-semicircle biochip, and interdigitate-zigzag biochip were 1573.2, 2081.3, and 2923.1, respectively, which can be defined as the measurements sensitivities.

By adding a semi-circle structure at the electrode edge of the interdigitate biochip, the edge of the WE and CE lengthened from 43.95 mm to 61.94 mm. According to a previously published paper [25], proportionally, the sensitivity should improve by about 18.2% from an interdigitate biochip to an interdigitate-semicircle biochip. However, the real sensitivity improvement measured was 32.3% (the slope of the trend line equation changed from 1573.2 to 2081.3) which was higher than the value of the deduction. By adding a zigzag structure at the electrode edge of the interdigitate biochip, the edge of WE and CE lengthened from 43.95 mm to 82.3 mm. The electrochemical measurement sensitivity should improve by about 38.8% from the interdigitate biochip to the interdigitate-zigzag biochip, however, the actual measured sensitivity improvement was higher at 85.81% (the slope of trend line equations changed from 1573.2 to 2923.1). The additional improvements both in the interdigitate-semicircle biochip (14.1%) and interdigitate-zigzag biochip (47.01%) were from the influence from the sharper structure at the electrode edge which resulted in a higher electrolyte density and better measurement efficiency. The electrolyte current density at the triangular tip was about 3.77 times larger than that at the round tip. The additional improvement of the interdigitate-zigzag biochip (47.01%) was 3.3 times larger than that of the interdigitate-semicircle biochip (14.1%). These increases in the proportion are similar. It was shown that the difference between the additional improvement of the interdigitate-semicircle biochip and the interdigitate-zigzag biochip was due to the difference in the electrolyte current density between the triangular tip and the semi-circle round tip.

3.4 Other applications of the interdigitate-zigzag biochip

In this paper, we worked on detecting CVD and used a CVD biomarker, CRP, as the

other model protein. To examine the developed zigzag electrode design which can be used for different cross-linkers, cysteamine was used.

The impedance data of the 4-ATP/glutaraldehyde/antiCRP/ETA&BSA modified electrode after the addition of the CRP at different concentrations in the Nyquist form is shown in Data in Brief Figure 1(d). As described above, an interaction between the anti-CRP and CRP resulted in a steric hindrance. The isoelectric point of the CRP was 5.45, which confirms that there was an electrostatic repulsive force between the CRP and the negatively charged redox species in a 1×PBS at pH 7.4. Therefore, the higher concentration of the CRP resulted in the higher steric hindrance and the higher electrostatic repulsive force. It is illustrated that the impedance change increased with increasing concentration of the CRP. Figure 5(d) shows the good logarithmic linear relationship between the R_{et} and the logarithm of the CRP concentration was found to be in the range between 5.9 pM and 58.9 nM, with the regression coefficient of 0.9707. The slopes of the trend line equations for S100 beta protein and CRP were 2923.1 and 640.02, respectively. The slopes of the trend line equations can be defined as the sensitivities. Thus, the sensitivity of CRP case was lower than that of S100 beta protein case. Although the molecular weight of CRP was larger than the S100 beta protein, the unit impedance change produced by the CRP was smaller than that produced by the S100 beta protein. On the other hand, the isoelectric point of the S100 beta protein and CRP obtained were 4.52 and 5.45, respectively. In a pH 7.4, 1×PBS, both the S100 beta protein and CRP were negatively charged. However, the S100 beta protein had a more negative charge due to the larger difference between the isoelectric point of the S100 beta protein and the pH value of the PBS. Therefore, there appeared to be a larger electrostatic repulsive force between the S100 beta protein and electrolytes than that between the CRP and the electrolyte. This is the main reason that the unit impedance change produced by S100 beta protein was larger than that produced by the CRP. These results demonstrate that the action of an electrolyte repulsive force is larger than that of steric hindrance and clearly shows that it dominates the electrochemical measurements in our detection architecture.

The impedance data of the cysteamine/glutaraldehyde/antibody/ETA&BSA modified electrode after the addition of the proteins at different concentrations in the Nyquist form are shown in Data in Brief Figure 1(e)(f). The impedance change increased with increasing concentration of the proteins due to the steric hindrance and electrostatic repulsive force in both the S100 beta protein and CRP cases. Figure 5(e) shows the good logarithmic linear relationship with the regression coefficient of 0.9843 and 0.9816 between ΔR_{et} and the logarithm of the concentrations. The slopes of the trend line equations for the S100 beta protein and CRP were 221.95 and 102.23, respectively. The slopes of the trend line equations can be defined as the sensitivities. Thus, for the cysteamine-based biochip, the sensitivity of the S100 beta protein case was higher than that of the CRP case, which is consistent with that of a 4-ATP-based biochip. Moreover, although the sensitivity of the cysteamine-based

biochip was lower than that of the 4-ATP-based biochip, the impedance change between two concentrations can be distinguished clearly. This indicates that the cysteamine-based biochip can also be suitable for detecting both S100 beta protein and CRP.

4. Conclusions

In this study, the sensitivity of electrochemical measurements was improved by using an interdigitate-zigzag biochip. Computer simulation was used to investigate several potential effective possibilities, and the results showed a higher electrolyte current density on a sharp tip at the edge near the WE and CE. We found that biomolecules bound near to the sharp tip can be detected easily and hence can improve measurement efficiency. Therefore, by adding a zigzag structure at the edge near the WE and CE without the changing the area of the WE and CE, a measurement sensitivity of the CVD biomarker was improved by 85.81%. Using a CVD biomarker, a S100 beta protein as a model protein, a logarithmic linear dynamic range from 27 pM (10 ng/ml) to 270 nM (10 μg/ml) was obtained, and the detection limit was 27 pM (10 ng/ml). For another CVD biomarker, CRP, a logarithmic linear dynamic range from 5.9 pM to 58.9 nM was obtained. Moreover, cysteamine was found to be the suitable linker in the interdigitate-zigzag biochip. We found that the new configuration has the potential to be an excellent PoC biosensor when used for the detection of CVD biomarkers. In the future, to further enhance sensitivity and performance of our new configuration, we can look at incorporating other improvements to the design which will allow it to meet any clinical concentration requirements.

Acknowledgements

The authors thank the Taiwan National Science Council for its support under Project No. MOST 103-2627-E-002-004

References:

[1] World Health Organization, http://www.who.int/en/.

[2] E. Imbalzano, G. Mandraffino, M. Casciaro, S. Quartuccio, A. Saitta, S. Gangemi, Pathophysiological mechanism and therapeutic role of S100 proteins in cardiac failure: a systematic review, Heart Failure Reviews 21 (2016) 463-473. http://dx.doi.org/10.1007/s10741-016-9529-8

[3] Frieder W Scheller, Ulla Wollenberger, Axel Warsinke, Fred Lisdat, Research and development in biosensors, Current Opinion in Biotechnology 12 (2001) 35-40. http://dx.doi.org/10.1016/S0958-1669(00)00169-5.

[4] J. V. Rushworth, N. A. Hirst, J. A. Goode, D. J. Pike, A. Ahmed, P. A. Millner, Impedimetric biosensors for medical applications: current progress and challenges,

Momentum Press (2013). http://dx.doi.org/10.1115/1.860243.

[5] J. C. Pickup, F. Hussain, N. D. Evans, O. J. Rolinski, D. J. Birch, Fluorescence-based glucose sensors, Biosensors and Bioelectronics 20 (2005) 2555-2565. http://dx.doi.org/10.1016/j.bios.2004.10.002

[6] J. Homola, Surface plasmon resonance sensors for detection of chemical and biological species, Chemical Reviews 108 (2008) 462-493. http://dx.doi.org/10.1021/cr068107d.

[7] A. Janshoff, H. J. Galla, C. Steinem, Piezoelectric Mass-Sensing Devices as Biosensors—An Alternative to Optical Biosensors? Angewandte Chemie International Edition 39 (2000) 4004-4032. http://dx.doi.org/10.1002/1521-3773(20001117)39:22<4004::AID-ANIE4004>3.0.CO;2-2

[8] Roberto Raiteri, Massimo Grattarola, Hans-Jürgen Butt, Petr Skládal, Micromechanical cantilever-based biosensors, Sensors and Actuators B: Chemical 79 (2001) 115-126. http://dx.doi.org/10.1016/S0925-4005(01)00856-5.

[9] M.V. Voinova, M. Jonson, B. Kasemo, 'Missing mass' effect in biosensor's QCM applications, Biosensors and Bioelectronics 17 (2002) 835-841. http://dx.doi.org/10.1016/S0956-5663(02)00050-7.

[10] Dorothee Grieshaber, Robert MacKenzie, Janos Vörös, Erik Reimhult, Electrochemical Biosensors - Sensor Principles and Architectures, Sensors 8 (2008) 1400-1458. http://dx.doi.org/10.3390/s80314000.

[11] J. Wang, Electrochemical Glucose Biosensors, Chemical Reviews 108 (2008) 814-825. http://dx.doi.org/10.1021/cr068123a.

[12] Chen, C. S., K. N. Chang, Y. H. Chen, C. K. Lee, B. Y. J. Lee, A. S. Y. Lee, "Development of a label-free impedance biosensor for detection of antibody–antigen interactions based on a novel conductive linker," *Biosensors and Bioelectronics,* vol. 26, pp. 3072-3076, 2011.

[13] G. A. Zelada-Guillén*, et al.*, "Ultrasensitive and real-time detection of proteins in blood using a potentiometric carbon-nanotube aptasensor," *Biosensors and Bioelectronics,* vol. 41, pp. 366-371, 2013.

[14] J. S. Daniels and N. Pourmand, "Label-Free Impedance Biosensors: Opportunities and Challenges," *Electroanalysis,* vol. 19, pp. 1239-1257, 2007.

[15] A. Bardea*, et al.*, "Sensing and amplification of oligonucleotide-DNA interactions by means of impedance spectroscopy: a route to a Tay-Sachs sensor," *Chemical Communications,* vol. 0, pp. 21-22, 1999.

[16] L. Yang and R. Bashir, "Electrical/electrochemical impedance for rapid detection of foodborne pathogenic bacteria," *Biotechnology Advances,* vol. 26, pp. 135-150, 2008.

[17] H. Chen*, et al.*, "An electrochemical impedance immunosensor with signal amplification based on Au-colloid labeled antibody complex," *Sensors and Actuators*

B: Chemical, vol. 117, pp. 211-218, 2006.

[18] X. Fang*, et al.*, "Integrated biochip for label-free and real-time detection of DNA amplification by contactless impedance measurements based on interdigitated electrodes," *Biosensors and Bioelectronics,* vol. 44, pp. 241-247, 2013.

[19] W. Olthuis*, et al.*, "Theoretical and experimental determination of cell constants of planar-interdigitated electrolyte conductivity sensors," *Sensors and Actuators B: Chemical,* vol. 24, pp. 252-256, 1995.

[20] P. Van Gerwen*, et al.*, "Nanoscaled interdigitated electrode arrays for biochemical sensors," *Sensors and Actuators B: Chemical,* vol. 49, pp. 73-80, 1998.

[21] J. Min and A. J. Baeumner, "Characterization and optimization of interdigitated ultramicroelectrode arrays as electrochemical biosensor transducers," *Electroanalysis,* vol. 16, pp. 724-729, 2004.

[22] S. K. Kim*, et al.*, "Fabrication of comb interdigitated electrodes array (IDA) for a microbead-based electrochemical assay system," *Biosensors and Bioelectronics,* vol. 20, pp. 887-894, 2004.

[23] K. Aoki*, et al.*, "Quantitative analysis of reversible diffusion-controlled currents of redox soluble species at interdigitated array electrodes under steady-state conditions," *Journal of electroanalytical chemistry and interfacial electrochemistry,* vol. 256, pp. 269-282, 1988.

[24] A. E. Cohen and R. R. Kunz, "Large-area interdigitated array microelectrodes for electrochemical sensing," *Sensors and Actuators B: Chemical,* vol. 62, pp. 23-29, 2000.

[25] Y.-C. Kuo*, et al.*, "Sensitivity improvement of a miniaturized label-free electrochemical impedance biosensor by electrode edge effect," *Journal of Micro/Nanolithography, MEMS, and MOEMS,* vol. 13, pp. 033019-033019, 2014.

Figure 1. (a) Interdigitate biochip; (b) Interdigitate-semicircle biochip; (c) Interdigitate-zigzag biochip; (d) The results of the electrolyte current density distribution simulation of the interdigitate biochip with 150-μm gap and 111.8-μm gap (e).

Figure 2. Electrolyte current density distribution simulation of single structure: (a) simulation model and electrolyte current density distribution of single semicircle structure, (b) electrolyte current density distribution curve of the black dashed line in (a), (c) simulation model and electrolyte current density distribution of single triangular structure, and (d) electrolyte current density distribution curve of the black dashed line in (c).

Figure 3. Electrolyte current density distribution simulation of the whole detection area of the biochip: (a) 20 mm × 25 mm biochip, (b) simulation model, (c) interdigitate biochip, (d)

interdigitate-semicircle biochip, and (e) interdigitate-zigzag biochip.

Figure 4. Results of electrolyte current density distribution simulation in three-dimensional space: (a) simulation model, (b) surface analysis, and (c) slice analysis.

Figure 5. (a) Process of the antibody-antigen interactions; (b) Randles circuit model; (c) Relationship between ΔRet and S100 beta protein concentrations from 27 pM to 270 nM on 4-ATP-based surface in the interdigitate biochip, interdigitate-semicircle biochip, and interdigitate-zigzag biochip; (d) Relationship between ΔRet and CRP concentrations from 5.9 pM to 58.9 nM on 4-ATP-based surface in interdigitate-zigzag biochip; (e) Relationship between ΔRet and S100 beta protein concentrations from 27 pM to 270 nM and relationship between ΔRet and CRP concentrations from 5.9 pM to 58.9 pM on cysteamine-based surface in interdigitate-zigzag biochip; (f) Summary of the slopes of the trend line equations (sensitivities) in all kinds of biochips.

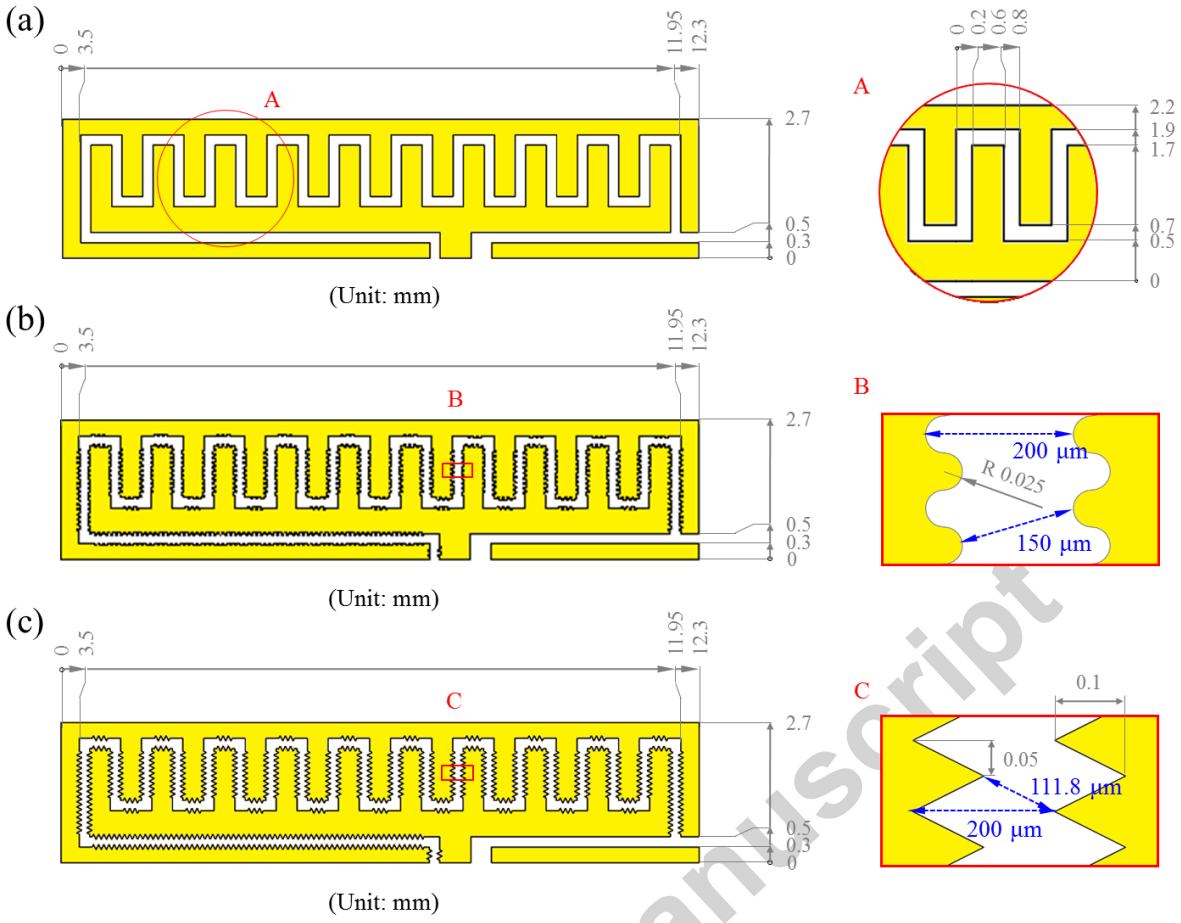

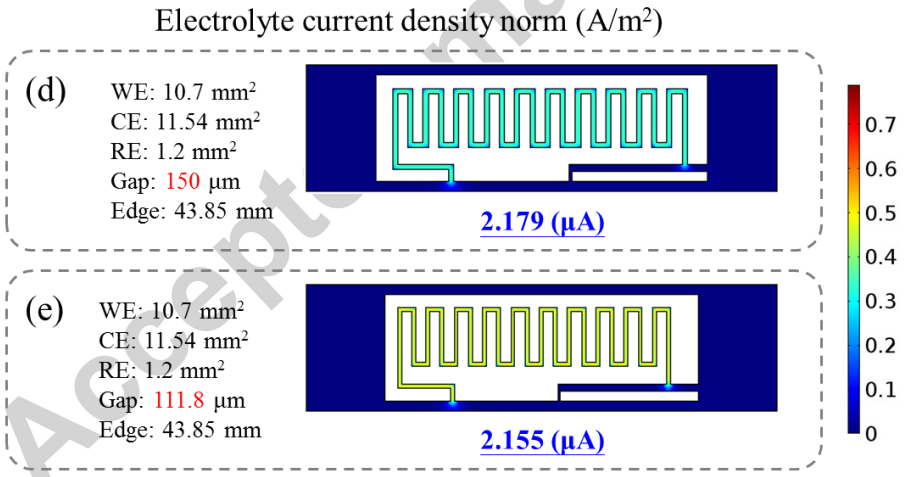

Figure 1

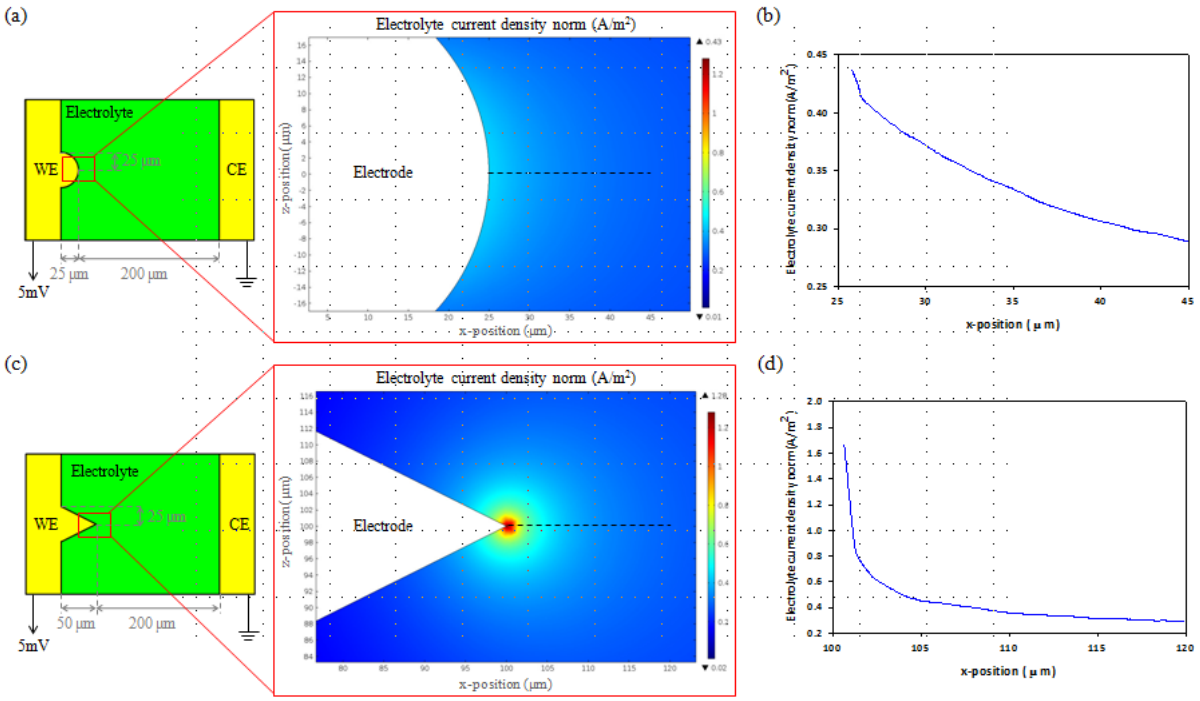

Figure 2

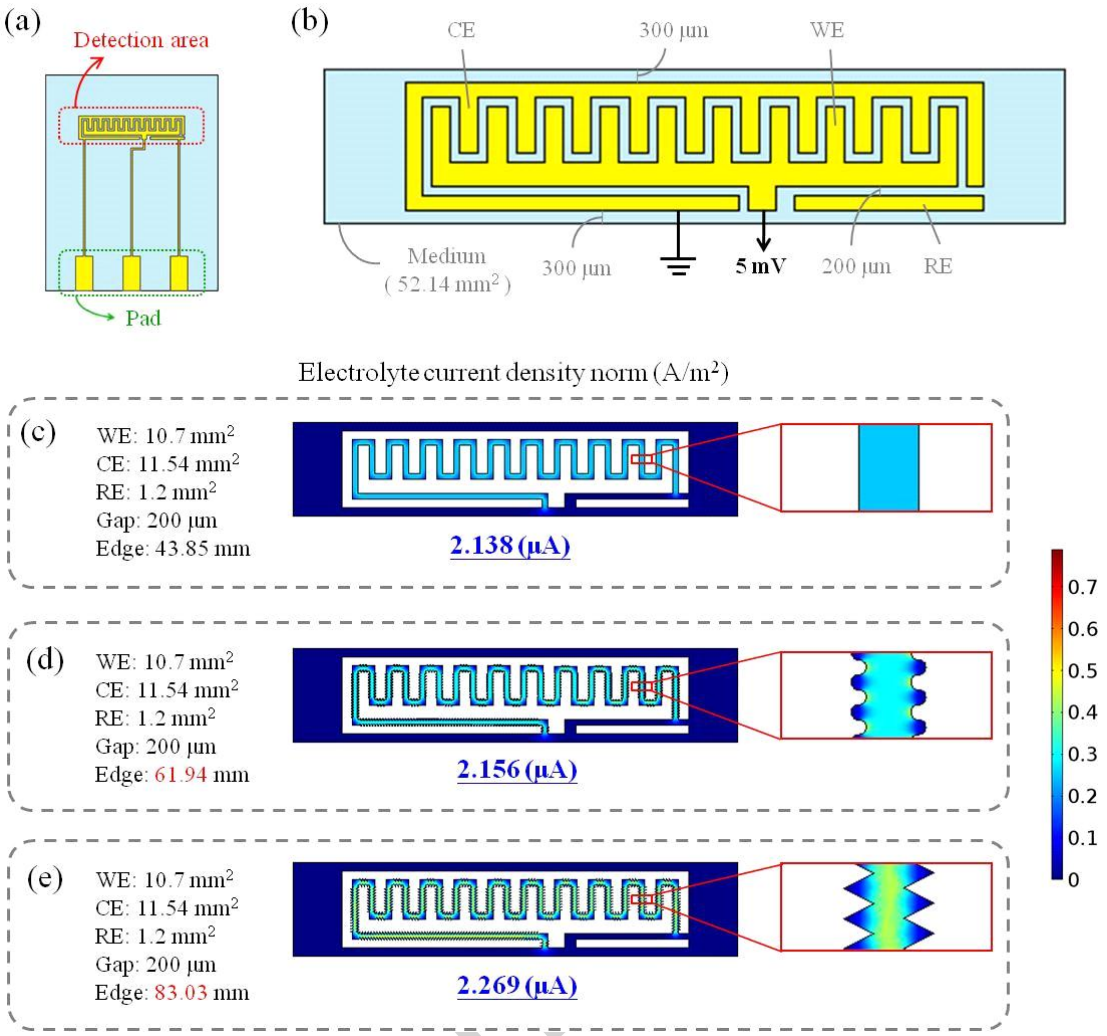

Figure 3

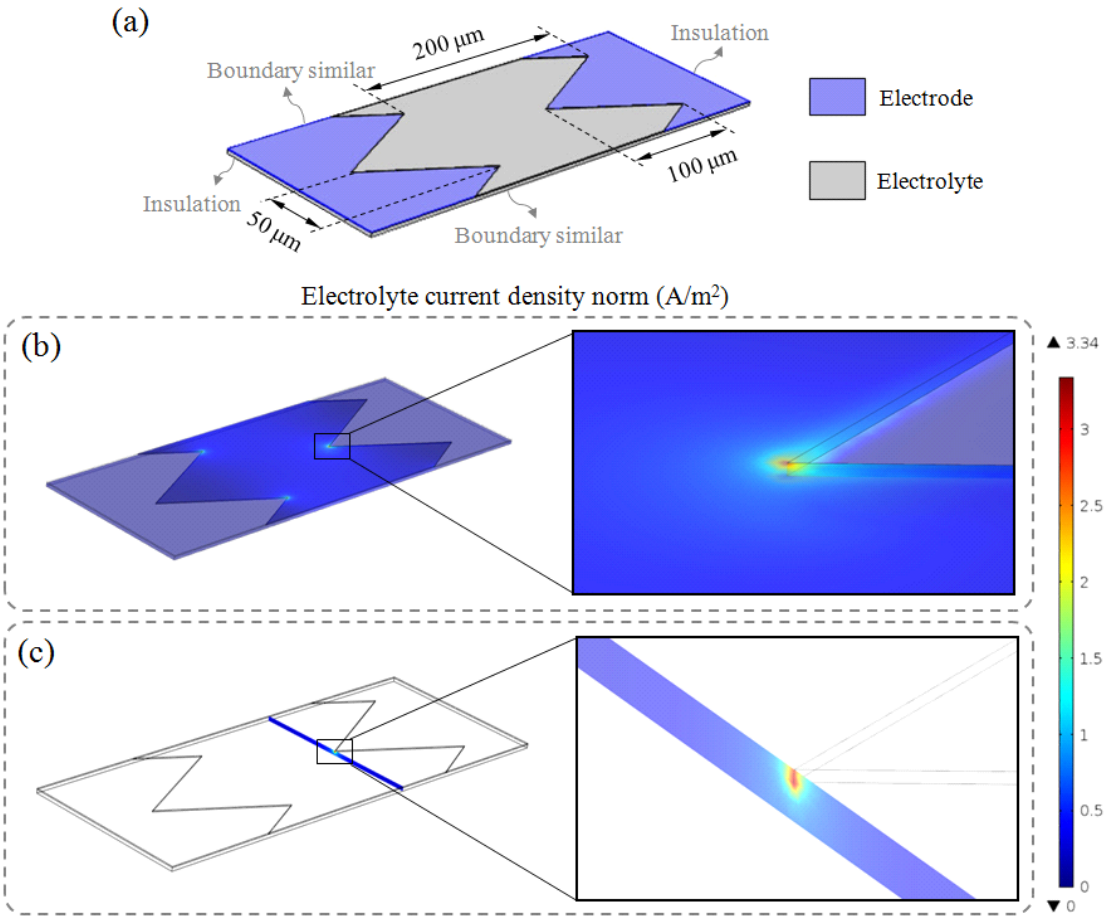

Figure 4

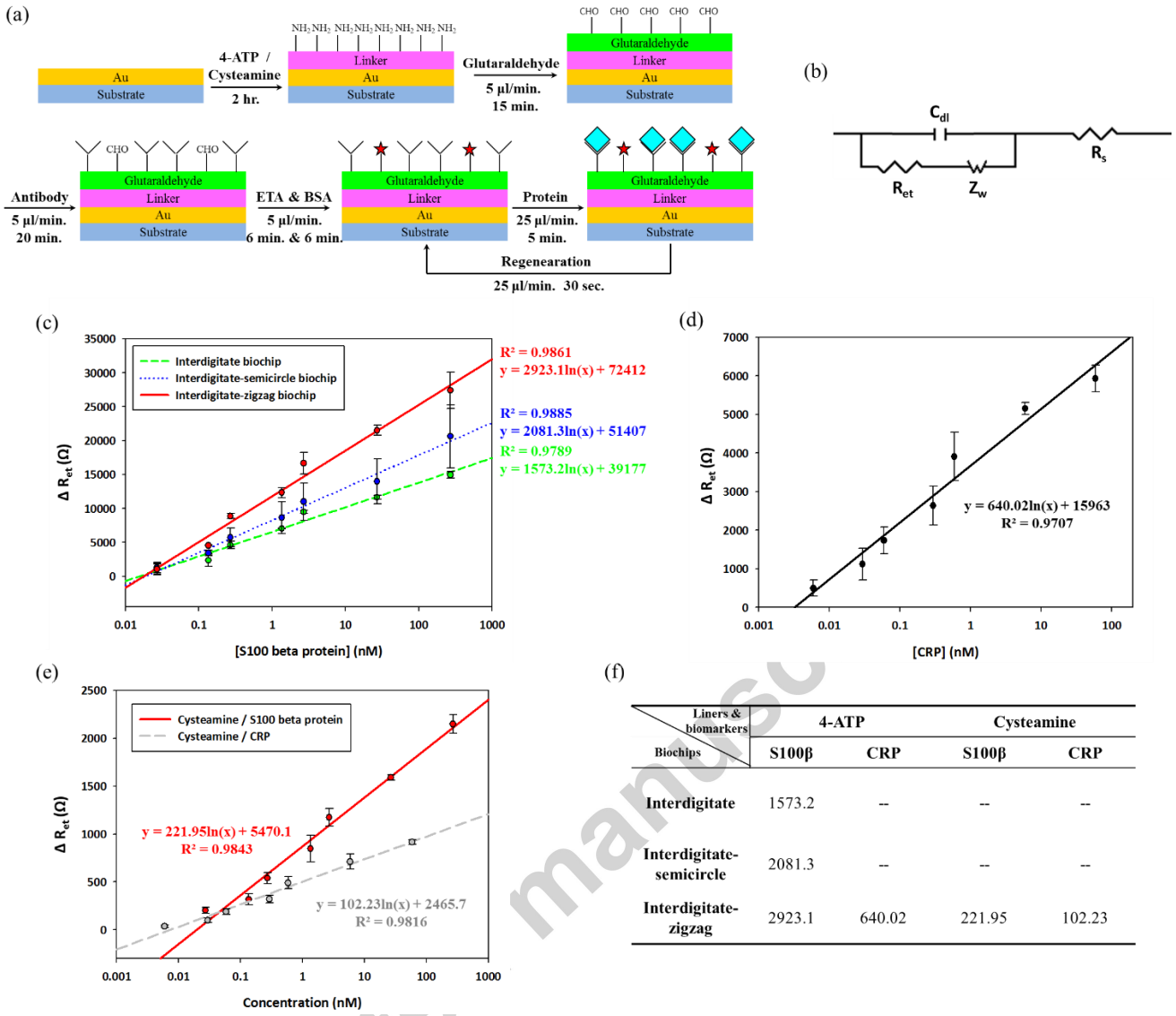

(f)

Liners & biomarkers / Biochips	4-ATP		Cysteamine	
	S100β	CRP	S100β	CRP
Interdigitate	1573.2	--	--	--
Interdigitate-semicircle	2081.3	--	--	--
Interdigitate-zigzag	2923.1	640.02	221.95	102.23

Figure 5

Table 1. (a) Molecular weight and structure of 4-ATP, cysteamine, glutaraldehyde, and ETA; (b) Details of S100 beta protein and CRP.

(a)

Name	Molecular weight	structure
4-ATP	125.19	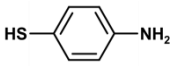
Cysteamine	77.15	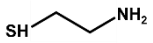
Glutaraldehyde	100.12	
ETA	97.54	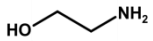

(b)

Name	Molecular weight	Isoelectric point
S100 beta protein	37 kDa	4.52
CRP	~115 kDa	5.45

Highlights:

- A zigzag structure was add to the electrode edge near the WE and CE due to the electrode point effect.
- The electrochemical measurement sensitivity was improved using an interdigitate-zigzag biochip.
- Our newly developed biochip design can detect CVD biomarkers such as S100 beta protein and CRP.
- CVD biomarkers can be detected not only on an ATP-based surface but also on a cysteamine-based surface.